High performance implementation and conceptual development of the wave based method for steady-state dynamic analysis of acoustic problems

B. van Hal[1], **A. Hepberger**[2], **H.-H. Priebsch**[2], **W. Desmet**[1], **P. Sas**[1]

[1] K.U.Leuven, Department of Mechanical Engineering,
Celestijnenlaan 300 B, B-3001, Heverlee, Belgium
e-mail: bas.vanhal@mech.kuleuven.ac.be,

[2] ACC Acoustic Competence Center G.m.b.H.,
Inffeldgasse 25, A-8010 Graz, Austria

Abstract

The *wave based method (WBM)* is considered for the steady-state dynamic analysis of *acoustic* problems as an alternative for the *finite element method (FEM)*. The *WBM* exhibits better convergence properties with respect to model sizes, but the computation (CPU) times obtained by the current MATLAB implementation are large compared to commercially available *FEM* codes. Recently, a *high performance* FORTRAN code has been developed, which becomes more efficient than the commercially available *FEM* codes, even with respect to the CPU times. Despite the good results presented in this paper, the conceptual development of the *WBM* still requires much attention. The following topics are discussed briefly: the domain decomposition, the extension of the expansion of basis functions, which forms the approximation solution, the boundary integration scheme and the coupling between the *FEM* and the *WBM*. The results of these investigation may improve the efficiency of the *high performance* FORTRAN implementation further.

1 Introduction

The *finite element method (FEM)* is a widely accepted prediction tool for the steady-state dynamic analysis of *acoustic* problems [1], [2]. However, the *FEM* is practically limited to the low-frequency application range, since the computational costs increase for increasing frequency. Recently, an alternative deterministic method has been developed, namely the *wave based method (WBM)* [3], which is based on the TREFFTZ approach [4]. The *WBM* exhibits better convergence properties with respect to model sizes than the *FEM*. Therefore, the frequency application range of the deterministic methods can be extended towards the mid-frequency range.

Until recently, the *WBM* has only been implemented in a MATLAB code. This results in longer computation (CPU) times than commercially available software. In order to demonstrate the capability of the *WBM* to be more efficient than the *FEM*, also with respect to CPU times, a *high performance* implementation is required. A recently developed FORTRAN code is well suited for this purpose. After a brief discussion of the theoretical background of the *WBM*, this paper demonstrates that the *high performance* implementation of the *WBM* is more efficient for a *2-dimensional (2D) uncoupled acoustic* benchmark problem than the commercially available *finite element* code SYSNOISE [5].

Despite the good results presented in this paper, more research is required. The model sizes in the *WBM* are smaller than in the *FEM*, but the system matrices are no longer sparse. This may cause memory problems in the *3D* case. Therefore, still much attention is given to the conceptual development of the method. This paper sheds some light on a few research topics. Most attention goes to the domain decomposition, which is required for the analysis of non-convex domains. Furthermore, the extension of the currently applied expansion of basis functions, which forms the approximation solution, the applied integration schemes and the coupling between the *FEM* and the *WBM* are discussed briefly.

2 Basic concept

2.1 Problem definition

Consider the *2D uncoupled acoustic* problem shown in figure 1. The *acoustic* domain Ω, surrounded by the boundary Γ, is excited by the cylindrical source q at position $\mathbf{r}_q$. The *Helmholtz* equation governs the steady-state pressure response, described by its complex amplitude p, at position $\mathbf{r} = (x, y)$

$$\left(\Delta + k^2\right) p(\mathbf{r}) = -j\rho\omega q\delta(R), \quad \forall\, \mathbf{r} \in \Omega, \tag{1}$$

where $\Delta = \partial^2/\partial x^2 + \partial^2/\partial y^2$ represents the Laplace operator, $k = \omega/c$ the wave number with the radial excitation frequency ω and the speed of sound c, ρ the ambient density, δ the Dirac delta function and $R = \|\mathbf{r} - \mathbf{r}_q\|$ the distance between the response point and excitation point. The boundary Γ is the union of the boundary Γ_p with the prescribed pressure $\bar{p}$, the boundary Γ_v with the prescribed normal velocity $\bar{v}_n$ and the boundary Γ_Z with the prescribed normal impedance $\bar{Z}$ ($\Gamma = \Gamma_p \cup \Gamma_v \cup \Gamma_Z$). The following relations describe the *acoustic* boundary conditions

$$\left\{ \begin{array}{rcll} \mathcal{L}_v(p) & = & \dfrac{p}{\bar{Z}}, & \text{at } \Gamma_{\mathrm{Z}}, \\ \mathcal{L}_v(p) & = & \bar{v}_n, & \text{at } \Gamma_{\mathrm{v}} \text{ and} \\ p & = & \bar{p}, & \text{at } \Gamma_{\mathrm{p}} \end{array} \right. \tag{2}$$

$$\text{with } \mathcal{L}_{\mathrm{v}} = \frac{\mathrm{j}}{\rho\omega}\frac{\partial}{\partial \mathrm{n}},$$

where $\partial/\partial n$ represents the derivative in the outward normal direction $\mathbf{n}$.

2.2 Pressure approximation

The pressure field p is approximated by an expansion of n_a wave functions Φ_a extended by a particular solution function $\hat{p}_q$. The pressure approximation $\hat{p}$ is given by

$$\begin{array}{rcccl} p(\mathbf{r}) \;\approx\; \hat{p}(\mathbf{r}) & = & \displaystyle\sum_{a=1}^{n_a} \Phi_a(\mathbf{r}) p_a & + & \hat{p}_q(\mathbf{r}) \\ & = & \boldsymbol{\Phi}^T(\mathbf{r})\mathbf{p} & + & \hat{p}_q(\mathbf{r}) \end{array} \tag{3}$$

where p_a represents the contribution of each wave function to the pressure approximation $\hat{p}$. The wave contributions p_a form the unknown *degrees of freedom* (*DOF's*) of the *wave model*. The wave functions Φ_a and the wave contributions p_a are stored, respectively, in the column vectors $\boldsymbol{\Phi}$ and $\mathbf{p}$. The ^{T} in (3) denotes the transpose operator.

The set of wave functions Φ_a is defined by

$$\begin{array}{l} \Phi_a(x, y) = \mathrm{e}^{-j(k_{a,x}x + k_{a,y}y)}, \\ \text{with } k_{a,x}^2 + k_{a,y}^2 = k^2. \end{array} \tag{4}$$

The above functions are homogeneous solutions of the governing *Helmholtz* equation. The free field pressure response to the cylindrical source q is selected as particular solution $\hat{p}_q$

$$\hat{p}_q(\mathbf{r}) = \frac{\rho\omega q}{4} H_0^{(2)}(kR), \tag{5}$$

with the zero-order Hankel function of the second kind $H_0^{(2)}$.

2.3 Wave model

The pressure approximation $\hat{p}$ satisfies a priori the governing *Helmholtz* equation (1), since it consists of a linear combination of homogeneous solutions extended by a particular solution. Therefore, the boundary conditions (2) determine the unknown wave contributions p_a. The *wave model* is obtained by enforcing the pressure approximation $\hat{p}$ to satisfy the boundary conditions (2) in an integral sense. The above procedure is performed either by applying a *weighted residual formulation* or a *least-squares formulation* of the boundary conditions.

2.3.1 Weighted residual formulation

In the *weighted residual formulation*, the violation of the boundary conditions is averaged to zero using a weighing function $\tilde{p}$ as follows

$$\int_{\Gamma_Z} \tilde{p} R_Z \,\mathrm{d}s + \int_{\Gamma_v} \tilde{p} R_v \,\mathrm{d}s - \int_{\Gamma_p} \mathcal{L}_v(\tilde{p}) R_p \,\mathrm{d}s = 0, \tag{6}$$

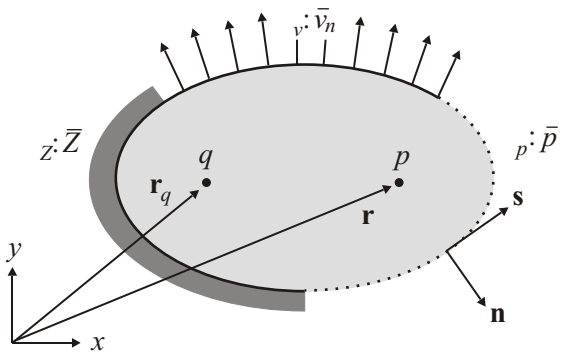

Figure 1: *2D coupled acoustic* problem

where s represents the boundary coordinate in tangential direction $\mathbf{s}$ (see figure 1) and where R_* represent the residual functions defined as

$$\begin{cases} R_Z &= \mathcal{L}_v(\hat{p}) - \dfrac{\hat{p}}{\bar{Z}}, & \text{at } \Gamma_{\mathrm{Z}}, \\ R_v &= \mathcal{L}_v(\hat{p}) - \bar{v}_n, & \text{at } \Gamma_{\mathrm{v}} \text{ and} \\ R_p &= \hat{p} - \bar{p}, & \text{at } \Gamma_{\mathrm{p}}. \end{cases} \tag{7}$$

By using each wave function Φ_a as a weighing function $\tilde{p}$, n_a linear equations are obtained, which form the following *wave model*

$$\mathbf{A}^{(WR)}\mathbf{p} = \mathbf{b}^{(WR)} \tag{8}$$

with the system matrix $\mathbf{A}^{(WR)}$ defined as

$$\begin{aligned} \mathbf{A}^{(WR)} = &\int_{\Gamma_Z} \mathbf{\Phi} \left(\mathcal{L}_v(\mathbf{\Phi}^T) - \tfrac{\mathbf{\Phi}^T}{\bar{Z}} \right) \mathrm{d}s + \dots \\ &\dots + \int_{\Gamma_v} \mathbf{\Phi} \mathcal{L}_v(\mathbf{\Phi}^T)\, \mathrm{d}s - \int_{\Gamma_p} \mathcal{L}_v(\mathbf{\Phi}) \mathbf{\Phi}^T\, \mathrm{d}s \end{aligned} \tag{9}$$

and with the system vector $\mathbf{b}^{(WR)}$ defined as

$$\begin{aligned} \mathbf{b}^{(WR)} = &- \int_{\Gamma_Z} \mathbf{\Phi} \left(\mathcal{L}_v(\hat{p}_q) - \tfrac{\hat{p}_q}{\bar{Z}} \right) \mathrm{d}s + \dots \\ &\dots + \int_{\Gamma_v} \mathbf{\Phi} \left(\bar{v}_n - \mathcal{L}_v(\hat{p}_q) \right) \mathrm{d}s + \dots \\ &\dots - \int_{\Gamma_p} \mathcal{L}_v(\mathbf{\Phi}) \left(\bar{p} - \hat{p}_q \right) \mathrm{d}s. \end{aligned} \tag{10}$$

2.3.2 Least-squares formulation

In the *least-squares formulation*, the violation of the boundary conditions is minimized along the boundary Γ. The following error functional

$$\begin{aligned} \mathcal{F} = &\alpha_v \int_{\Gamma_Z} \|R_Z\|^2 \mathrm{d}s + \dots \\ &\dots + \alpha_v \int_{\Gamma_v} \|R_v\|^2 \mathrm{d}s + \alpha_p \int_{\Gamma_p} \|R_p\|^2 \mathrm{d}s, \end{aligned} \tag{11}$$

which is a measure for the approximation error, is minimized with respect to the wave contributions p_a. This results in n_a linear equations of the following *wave model*

$$\mathbf{A}^{(LS)}\mathbf{p} = \mathbf{b}^{(LS)} \tag{12}$$

with the system matrix $\mathbf{A}^{(LS)}$ defined as

$$\begin{aligned} &\mathbf{A}^{(LS)} = ... \\ &\alpha_v \int_{\Gamma_Z} \left(\mathcal{L}_v^c(\mathbf{\Phi}^c) - \tfrac{\mathbf{\Phi}^c}{\bar{Z}^c} \right) \left(\mathcal{L}_v(\mathbf{\Phi}^T) - \tfrac{\mathbf{\Phi}^T}{\bar{Z}} \right) \mathrm{d}s + \dots \\ &\dots + \alpha_v \int_{\Gamma_v} \mathcal{L}_v^c(\mathbf{\Phi}^c) \mathcal{L}_v(\mathbf{\Phi}^T) \mathrm{d}s + \alpha_p \int_{\Gamma_p} \mathbf{\Phi}^c \mathbf{\Phi}^T \mathrm{d}s \end{aligned} \tag{13}$$

and with the system vector $\mathbf{b}^{(LS)}$ defined as

$$\begin{aligned} &\mathbf{b}^{(LS)} = ... \\ &-\alpha_v \int_{\Gamma_Z} \left(\mathcal{L}_v^c(\mathbf{\Phi}^c) - \tfrac{\mathbf{\Phi}^c}{\bar{Z}^c} \right) \left(\mathcal{L}_v(\hat{p}_q) - \tfrac{\hat{p}_q}{\bar{Z}} \right) \mathrm{d}s + \dots \\ &\dots + \alpha_v \int_{\Gamma_v} \mathcal{L}_v^c(\mathbf{\Phi}^c) \left(\bar{v_n} - \mathcal{L}_v(\hat{p}_q) \right) \mathrm{d}s + \dots \\ &\dots + \alpha_p \int_{\Gamma_p} \mathbf{\Phi}^c \left(\bar{p} - \hat{p}_q \right) \mathrm{d}s \end{aligned} \tag{14}$$

where ^{c} denotes the complex conjugate operator. The parameters α_v and α_p in (11) restore the homogeneity between the different components of the error functional $\mathcal{F}$. In the numerical experiments $\alpha_p = 1$ and $\alpha_v = (\rho c)^2$ are used.

2.3.3 Model properties

The *wave models*, discussed here, exhibit the following properties. The system matrices $\mathbf{A}^{(WR)}$ and $\mathbf{A}^{(LS)}$ are

- small compared to *finite element* models,
- fully populated and complex,
- implicitly dependent on frequency and
- symmetric and Hermitian, respectively.

The consequence of the implicit frequency dependency of the system matrices is that they cannot be assembled from frequency independent matrices as in the *FEM*. This feature disables the application of a modal superposition strategy.

2.4 Wave function selection

In order for the *WBM* to converge towards the exact solution, the set of wave functions in (4) has to be complete. The complex exponential functions in (4) can be combined to obtain the following two sets of wave functions

$$\Phi_a : \begin{cases} \Phi_r = \cos(k_{r,x}x) \mathrm{e}^{-jk_{r,y}y}, \ (r - \text{set}) \\ \Phi_s = \mathrm{e}^{-jk_{s,x}x} \cos(k_{s,y}y), \ (s - \text{set}) \end{cases} \tag{15}$$

with the wave numbers $\mathbf{k}_a = (k_{a,x}, k_{a,y})$ with $a = r, s$ defined as

$$\begin{aligned} \mathbf{k}_r &= \left(\frac{r\pi}{L_x}, \pm\sqrt{k^2 - k_{r,x}^2} \right), \ \forall r = 0, 1, \dots, n_r \\ \mathbf{k}_s &= \left(\pm\sqrt{k^2 - k_{s,y}^2}, \frac{s\pi}{L_y} \right), \ \forall s = 0, 1, \dots, n_s \end{aligned} \tag{16}$$

where L_x and L_y represent the dimensions of the smallest enclosing bounding box, around the problem domain Ω, as illustrated in figure 2. The number of DOF's of the *wave model* is $n_a = 2(n_r + 1) + 2(n_s + 1)$. The pressure approximation $\hat{p}$, based on these wave function sets, converges [3].

Finally, only a finite number of wave functions n_a can be applied. This requires the truncation of the r-set and the s-set, which is wave number k dependent according to the following truncation rule

$$n_r = \left\lceil T\frac{kL_x}{\pi} \right\rceil \quad \text{and} \quad n_s = \left\lceil T\frac{kL_y}{\pi} \right\rceil \qquad (17)$$

where $\lceil\ \rceil$ represents the round operator to the nearest integer towards infinity and T a user defined truncation parameter.

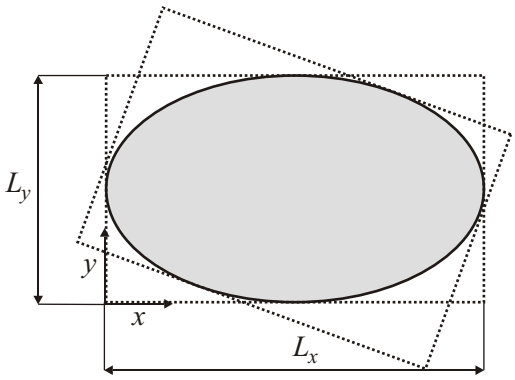

Figure 2: Smallest enclosing bounding box

3 High performance implementation

3.1 Benchmark problem

Consider the benchmark problem shown in figure 3, which is introduced for the comparison of the prediction results obtained by the *WBM* and the *FEM*. It consists of a *2D acoustic* cavity resembling a simplified car cavity. The vertical panel at $x = 0\ m$ excites the system with a unity velocity distribution. The remaining walls are either rigid or the normal impedance is prescribed by $\bar{Z} = -10\rho c$. The ambient density and the speed of sound in the cavity are respectively $\rho = 1.2\ kg/m^3$ and $c = 344\ m/s$.

3.2 *FRF* prediction

Before performing a detailed convergence analysis, the global dynamic behaviour of the *2D acoustic* system is predicted. At positions 1 and 2 (see figure 3)

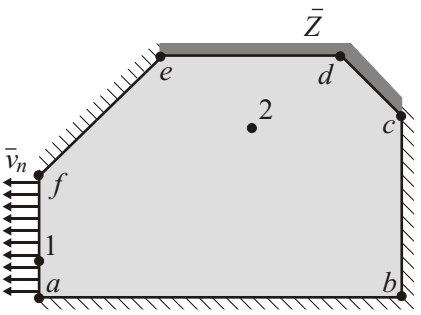

ID	x in m	y in m
a	0.00	0.00
b	1.50	0.00
c	1.50	0.75
d	1.25	1.00
e	0.50	1.00
f	0.00	0.50
1	0.00	0.15
2	0.88	0.70

Figure 3: Benchmark problem - *2D acoustic* cavity

the pressure *frequency response functions (FRF's)* are computed, which are visualized in respectively figures 4 and 5. These figures show the results of the *WBM* based on both the *weighted residual (WR)* formulation and the *least-squares (LS)* formulation with

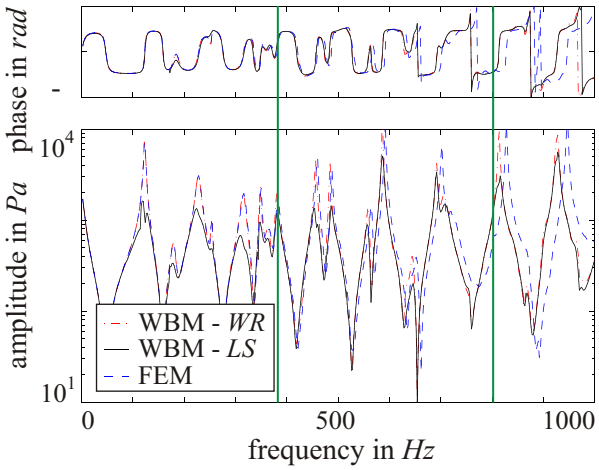

Figure 4: Pressure FRF at position 1

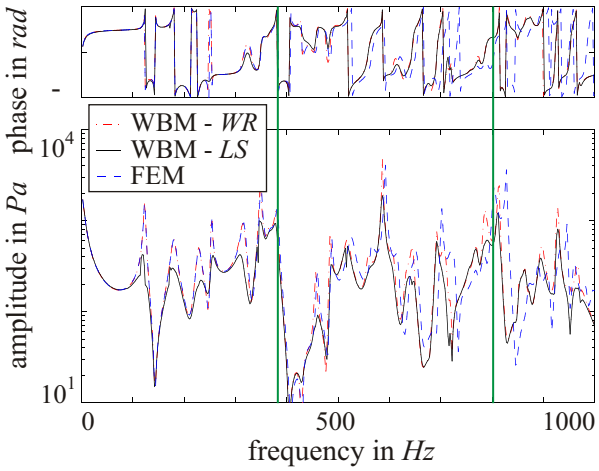

Figure 5: Pressure FRF at position 2

the truncation parameter $T = 2$. Furthermore, the pressure *FRF's* are presented, which are obtained by the *FEM* with a model of 540 *DOF's* constructed with linear quadrilateral elements. In the low-frequency range, containing the first few resonance frequencies, the *LS* formulation of the *WBM* is less efficient than the *WR* formulation. This effect is observed in [3] too.

A major advantage of the *WBM* is that it exhibits almost no pollution errors caused by numerically introduced dispersion. Even in the mid-frequency range, containing already many resonance frequencies, the resonance frequencies do not shift to higher frequencies as in case of the *FEM* [6]. This advantageous feature is confirmed by the validation of the numerical prediction results by measurements for a similar *3D acoustic* problem [7].

Regarding the pollution error, the rule of thumb [5], which states that at least 6 elements per wavelength are needed for an accurate prediction, is not satisfactory anymore for the mid-frequency applications. The maximum applicable frequency, defined as

$$f_{\max}^{(1)} = \frac{c}{6h_{\max}} \tag{18}$$

with the maximal element size $h_{\max}$, is approximately $f_{\max}^{(1)} \approx 570\ Hz$ for the *finite element* model of 540 *DOF's*. However, figures 4 and 5 indicate that at $500\ Hz$ already some pollution errors occur. A more conservative approximation of the maximum applicable frequency is given by [6]

$$f_{\max}^{(2)} = \frac{c}{6\sqrt[3]{h_{\max}^2 L}} \tag{19}$$

with the characteristic domain dimension L. For the considered benchmark problem this results in approximately $f_{\max}^{(2)} \approx 220\ Hz$ using $L = 1.7\ m$.

3.3 Convergence analysis

The convergence rate of the *WBM* and the *FEM* are compared for two distinct frequencies, namely for $f = 380\ Hz$ and $f = 800\ Hz$ (vertical cursors in figures 4 and 5). Figures 6 and 7 show the different convergence curves at positions 1 and 2 (denoted by point 1 and point 2). The relative pressure differences with respect to some reference solutions are plotted as function of either the number of *DOF's* or the required CPU time. The reference solutions for the pressure difference calculations are obtained by *wave models* with either $n_a = 338$ or $n_a = 704$ for respectively $f = 380\ Hz$ or $f = 800\ Hz$. Only the *WR* formulation of the *WBM* is considered.

The results of the MATLAB implementation and the *high performance* FORTRAN implementation of the *WBM* are compared to the *FEM* results obtained

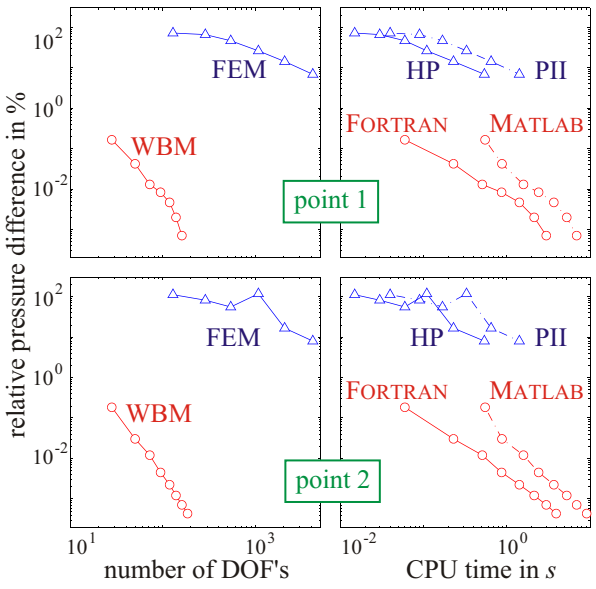

Figure 6: Convergence curves for $f = 380\ Hz$

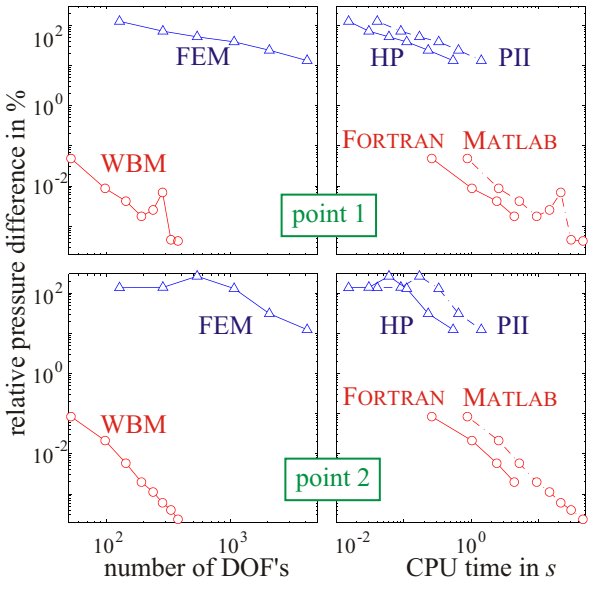

Figure 7: Convergence curves for $f = 800\ Hz$

code	processor
MATLAB	$650\ MHz$ Celeron
FORTRAN	$500\ MHz$ Pentium III
SYSNOISE	$400\ MHz$ HP-C3000 Unix
SYSNOISE	$450\ MHz$ Pentium II

Table 1: Computation details for convergence analysis (see figures 6 and 7)

by SYSNOISE REV 5.5 [5] (see table 1 for details). With respect to the number of *DOF's*, the *WBM* is far more efficient than the *FEM*. The relative pressure differences are at least two orders of magnitude smaller and the inclination of the convergence curves is steeper. With respect to the CPU times, the *WBM* is still more efficient than the *FEM*. The error levels are at least two orders of magnitude lower for a similar amount of computation time. The *high performance* FORTRAN implementation is two to three times faster than the MATLAB implementation. Furthermore, the efficiency of the FORTRAN implementation can be increased further by incorporating the improvements resulting from the conceptual development, which is the topic of section 4.

The convergence behaviour of both methods depends on the response position. The global error level is similar for the considered response position, but the slope of the convergence curves differ.

4 Conceptual development

4.1 Domain decomposition

4.1.1 Motivation

A sufficient condition for the *WBM* to converge is that the considered domain is convex [3]. However, this is not the case for most practical engineering problems. Therefore, a domain decomposition procedure has to be incorporated in the *WBM*. The theoretical background of the domain decomposition will be discussed briefly and its accuracy will be verified using the benchmark problem of an *L-shaped* domain.

4.1.2 Theoretical background

Consider the non-convex *2D acoustic* cavity in figure 8. The domain is splitted in two convex subdomains Ω_1 and Ω_2. The boundary Γ_b of each subdomain Ω_b is the union of the boundary Γ_{bp} with the prescribed pressure $\bar{p}_b$, the boundary Γ_{bv} with the prescribed normal velocity $\bar{v}_{bn}$, the boundary Γ_{bZ} with the prescribed normal impedance $\bar{Z}_b$ and the interface Γ_{bi} ($\Gamma_b = \Gamma_{bp} \cup \Gamma_{bv} \cup \Gamma_{bZ} \cup \Gamma_{bi}$). The boundary conditions at $\Gamma_b \backslash \Gamma_{bi}$ are defined in (2). The interface conditions for the two subdomains are given by

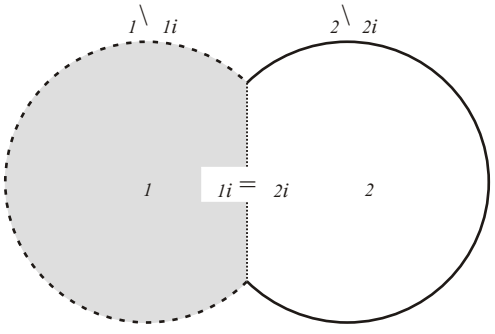

Figure 8: Domain decomposition

$$\begin{aligned} & p_1 = p_2, && \text{at } \Gamma_{1i} \\ \text{and} \quad & \mathcal{L}_{2v}(p2) = -\mathcal{L}_{1v}(p_1), && \text{at } \Gamma_{2i} \\ \text{with} \quad & \mathcal{L}_{bv} = \frac{j}{\rho\omega}\frac{\partial}{\partial n_b} \end{aligned} \tag{20}$$

where p_b represents the pressure in subdomain Ω_b and $\partial/\partial n_b$ the derivative in the outward-normal direction $\mathbf{n}_b$ of subdomain Ω_b.

The pressure p_b is approximated by the pressure approximation function $\hat{p}_b$ discussed in section 2.2. The *wave model* is obtained by enforcing the pressure approximation $\hat{p}_b$ to satisfy both the boundary conditions (2) and the interface conditions (20) in an integral sense. The *wave model* of the two coupled *acoustic* subdomains is given by

$$\begin{bmatrix} \mathbf{A}_1 + \mathbf{C}_{11} & \mathbf{C}_{12} \\ \mathbf{C}_{21} & \mathbf{A}_2 + \mathbf{C}_{22} \end{bmatrix} \begin{Bmatrix} \mathbf{p}_1 \\ \mathbf{p}_2 \end{Bmatrix} = \ldots \\ \ldots = \begin{Bmatrix} \mathbf{b}_1 + \mathbf{c}_{11} + \mathbf{c}_{12} \\ \mathbf{b}_2 + \mathbf{c}_{21} + \mathbf{c}_{22} \end{Bmatrix} \tag{21}$$

with the unknown wave contributions p_{ba}stored in the column vectors $\mathbf{p}_b$. The uncoupled system matrices $\mathbf{A}_b$ and vectors $\mathbf{b}_b$ are defined either by respectively equation (9) and (10) for the *WR* formulation or by respectively equation (13) and (14) for the *LS* formulation. The derivation of the coupling matrices $\mathbf{C}$ and coupling vectors $\mathbf{c}$ is similar to the derivation of the uncoupled system matrices and vectors as discussed in section 2.3. In case of the *WR* formulation the coupling matrices are defined as

$$\begin{aligned} \mathbf{C}_{11}^{(WR)} &= -\int_{\Gamma_{1i}} \mathcal{L}_{1v}(\mathbf{\Phi}_1)\, \mathbf{\Phi}_1^T \, \mathrm{d}s_1, \\ \mathbf{C}_{12}^{(WR)} &= \int_{\Gamma_{1i}} \mathcal{L}_{1v}(\mathbf{\Phi}_1)\, \mathbf{\Phi}_2^T \, \mathrm{d}s_1, \\ \mathbf{C}_{21}^{(WR)} &= \int_{\Gamma_{2i}} \mathbf{\Phi}_2\, \mathcal{L}_{1v}(\mathbf{\Phi}_1^T) \, \mathrm{d}s_2, \\ \mathbf{C}_{22}^{(WR)} &= \int_{\Gamma_{2i}} \mathbf{\Phi}_2\, \mathcal{L}_{2v}(\mathbf{\Phi}_2^T) \, \mathrm{d}s_2, \end{aligned} \tag{22}$$

where s_b represents the boundary coordinate in the tangential direction $\mathbf{s}_b$ of subdomain Ω_b. The cou-

pling vectors are defined as

$$\begin{aligned}
\mathbf{c}_{11}^{(WR)} &= \int_{\Gamma_{1i}} \mathcal{L}_{1v}(\mathbf{\Phi}_1)\, \hat{p}_{1q}\, \mathrm{d}s_1, \\
\mathbf{c}_{12}^{(WR)} &= -\int_{\Gamma_{1i}} \mathcal{L}_{1v}(\mathbf{\Phi}_1)\, \hat{p}_{2q}\, \mathrm{d}s_1, \\
\mathbf{c}_{21}^{(WR)} &= -\int_{\Gamma_{2i}} \mathbf{\Phi}_2\, \mathcal{L}_{1v}(\hat{p}_{1q})\, \mathrm{d}s_2, \\
\mathbf{c}_{22}^{(WR)} &= -\int_{\Gamma_{2i}} \mathbf{\Phi}_2\, \mathcal{L}_{2v}(\hat{p}_{2q})\, \mathrm{d}s_2.
\end{aligned} \tag{23}$$

In case of the *LS* formulation the coupling matrices are defined as

$$\begin{aligned}
\mathbf{C}_{11}^{(LS)} &= \alpha_{1p} \int_{\Gamma_{1i}} \mathbf{\Phi}_1^c\, \mathbf{\Phi}_1^T\, \mathrm{d}s_1, \\
\mathbf{C}_{12}^{(LS)} &= -\alpha_{1p} \int_{\Gamma_{1i}} \mathbf{\Phi}_1^c\, \mathbf{\Phi}_2^T\, \mathrm{d}s_1, \\
\mathbf{C}_{21}^{(LS)} &= \alpha_{2v} \int_{\Gamma_{2i}} \mathcal{L}_{2v}^c(\mathbf{\Phi}_2^c)\, \mathcal{L}_{1v}(\mathbf{\Phi}_1^T)\, \mathrm{d}s_2, \\
\mathbf{C}_{22}^{(LS)} &= \alpha_{2v} \int_{\Gamma_{2i}} \mathcal{L}_{2v}^c(\mathbf{\Phi}_2^c)\, \mathcal{L}_{2v}(\mathbf{\Phi}_2^T)\, \mathrm{d}s_2
\end{aligned} \tag{24}$$

and the coupling vectors as

$$\begin{aligned}
\mathbf{c}_{11}^{(LS)} &= -\alpha_{1p} \int_{\Gamma_{1i}} \mathbf{\Phi}_1^c\, \hat{p}_{1q}\, \mathrm{d}s_1, \\
\mathbf{c}_{12}^{(LS)} &= \alpha_{1p} \int_{\Gamma_{1i}} \mathbf{\Phi}_1^c\, \hat{p}_{2q}\, \mathrm{d}s_1, \\
\mathbf{c}_{21}^{(LS)} &= -\alpha_{2v} \int_{\Gamma_{2i}} \mathcal{L}_{2v}^c(\mathbf{\Phi}_2^c)\, \mathcal{L}_{1v}(\hat{p}_{1q})\, \mathrm{d}s_2, \\
\mathbf{c}_{22}^{(LS)} &= -\alpha_{2v} \int_{\Gamma_{2i}} \mathcal{L}_{2v}^c(\mathbf{\Phi}_2^c)\, \mathcal{L}_{2v}(\hat{p}_{2q})\, \mathrm{d}s_2.
\end{aligned} \tag{25}$$

4.1.3 Benchmark problem

The accuracy of the domain decomposition is verified using the benchmark problem of the *2D L-shaped* domain shown in figure 9. The *acoustic* system is excited by a uniform prescribed normal velocity of $\bar{v}_n = 1\ m/s$ at the horizontal wall at $y = 2\ m$. The remaining walls are rigid except for the vertical wall at $x = 4\ m$, where the normal impedance is prescribed by $\bar{Z} = -\rho c$ with $\rho = 1.2\ kg/m^3$ and $c = 344\ m/s$. Two response points are considered (see figure 9).

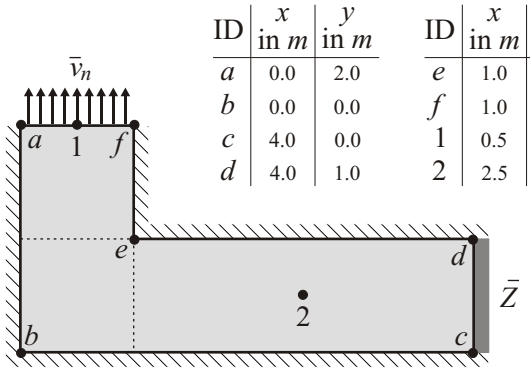

ID	x in m	y in m	ID	x in m	y in m
a	0.0	2.0	e	1.0	1.0
b	0.0	0.0	f	1.0	2.0
c	4.0	0.0	1	0.5	2.0
d	4.0	1.0	2	2.5	0.5

Figure 9: Benchmark problem - *2D L-shaped* domain

The *WBM* requires the division of the domain in subdomains, e.g. in three subdomains as illustrated in figure 9. Only the *WR* formulation of the *WBM* is considered here, since it is expected to be more efficient than the *LS* formulation.

A first verification of the accuracy follows from the comparison of the pressure *FRF* predictions obtained by the *WBM* with the truncation parameter $T = 2$ and the *FEM* with a model of 369 *DOF's* constructed with linear quadrilateral elements (see figures 10 and 11). In the low-frequency range the predictions of both methods coincide, but in the mid-frequency range the *FEM* results suffer from the pollution errors. The pollution errors are more pro-

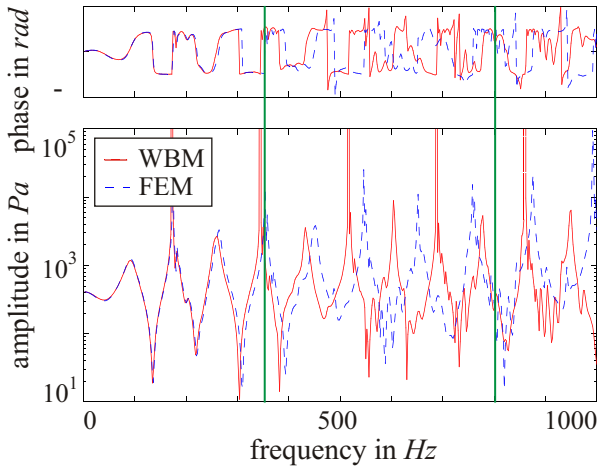

Figure 10: Pressure FRF at position 1

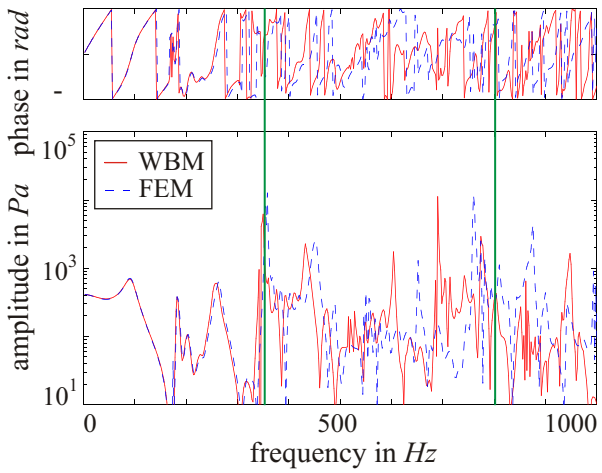

Figure 11: Pressure FRF at position 2

nounced for the benchmark problem of the *L-shaped* domain than the benchmark problem considered in section 3. The rule of thumb predicts the maximal application frequency of approximately $f^{(1)}_{\max} \approx 320\ Hz$ instead of $f^{(1)}_{\max} \approx 570\ Hz$ for the previous benchmark problem. The more conservative approximation gives $f^{(2)}_{\max} \approx 130\ Hz$, which is in this case more realistic since it takes into account the slender shape of the domain by the characteristic length parameter L. Despite the numerically introduced dispersion in the *FEM*, the comparison of the pressure *FRF* predictions indicate the high accuracy of the *WBM*.

Another way to verify the accuracy is to check the fulfillment of the boundary conditions and the interface conditions. This can be done qualitatively for the rigid walls and the interface by visual inspection of the pressure distribution. Consider the real part of the pressure distribution for $804\ Hz$ (mid-frequency range) shown in figure 12. The pressure contour lines are perpendicular to the rigid walls (where the normal derivative of the pressure is zero) and the pressure contour lines and their derivatives are continuous over the interfaces.

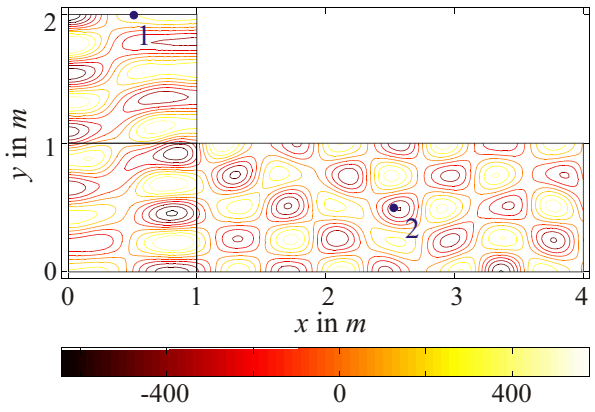

Figure 12: Real part of pressure distribution in Pa for $804\ Hz$

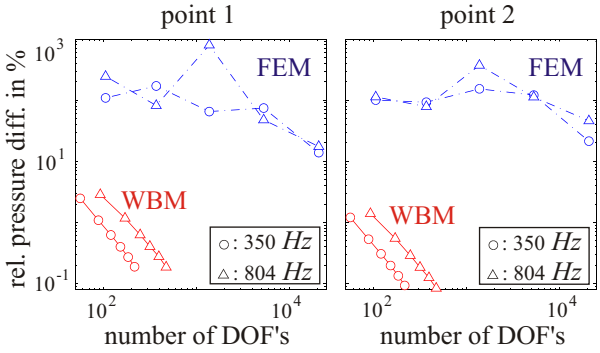

Figure 13: Convergence curves

Finally the accuracy is verified by a convergence analysis. The convergence rate of the *WBM* and the *FEM* are compared for two distinct frequencies, namely for $f = 350\ Hz$ and $f = 804\ Hz$ (vertical cursors in figures 10 and 11). Figure 13 shows the different convergence curves at response points 1 and 2. The relative pressure difference is plotted as function of the number of *DOF's*. The reference solutions for the pressure difference calculation are obtained by *wave models* with either $n_a = 796$ or $n_a = 1816$ for respectively $f = 350\ Hz$ or $f = 804\ Hz$. The comparison of the convergence curves shows that the *WBM* is far more efficient than the *FEM*, also in case of domain decomposition. The *FEM* results have not converged yet (more than 10% relative pressure difference). The error levels of the *WBM* predictions are at least two orders of magnitude lower for a similar amount of CPU time and the inclination of the convergence curves is steeper.

4.2 Wave function set

As mentioned in section 3.2 the *WBM* becomes more efficient past the low-frequency application range, certainly for the *LS* formulation. However, it should be mentioned that for rectangular domains both the *WR* and the *LS* formulation of the *WBM* show superconvergent behaviour [8]. The *LS* formulation suffers most from the lack of accuracy in case of domains with arbitrary geometries for the low resonance frequencies (see figures 4 and 5). The reason for this is that the current wave function set (15) cannot approximate the standing wave behaviour at the low resonance frequencies efficiently. The set of basis functions contains only a few propagating wave functions, which will contribute most to the standing wave pattern. E.g. consider the wave numbers of the r-set (16). A wave function Φ_r is propagating if $k_{r,y}$ is a real number, otherwise Φ_r is evanescent in the y-direction. E.g. in case of the *2D acoustic* benchmark problem, considered in section 3, the wave functions with $r > 3$ are evanescent for $f = 380\ Hz$ and the total number of propagating wave functions is 14, which is the number of propagating wave functions already obtained for a truncation parameter $T = 1$.

In general, model refinement consists of primarily adding evanescent wave functions. The extension of the wave function set with additional propagating wave functions may improve the computational efficiency of the method. In [8] some extensions of the current wave function set are proposed, which are summarized here.

1. Apply more independent enclosing bounding boxes than the smallest enclosing one for the construction of the wave function set (see figure 2).

2. Extend the current wave function set by only the propagating waves based on other independent enclosing bounding boxes.

3. Double the number of propagating wave functions based on the smallest enclosing bounding box. This requires a modification of relation (16).

The verification experiments, performed on a simple *2D uncoupled acoustic* problem, show that only the third proposal slightly improves the efficiency of the *WBM* based on the *LS* formulation. However, more verification experiments are required on *coupled acoustic* problems to investigate the capabilities of the proposed extensions to improve the computational efficiency.

4.3 Integration scheme

The construction of a *wave model* involves the evaluation of complex boundary integrals (see e.g. equations (9) and (10)). In general, these evaluations are performed numerically by the application of a GAUSS integration scheme [9]. However, due to the high oscillatory behaviour of the integrand, which increases for increasing frequency, many GAUSS points are required. This results in large computational efforts for constructing a *wave model*.

Fortunately, the integrals, which involve functions of the wave functions $\mathbf{\Phi}$, can be solved analytically, when the boundary geometry is either restricted to or approximated as a union of straight curves. This procedure has been applied to the generation of *structural wave models* [10] using the MATLAB code. The number of floating-point operations decreases significantly, but the used CPU time increases due to various conditional control statements (if-then-else) needed, which slow down the MATLAB code drastically. The FORTRAN programming language may suffer less from the lack of computational efficiency due to conditional control statements. Therefore, the application of the analytical solution functions of boundary integrals instead of the GAUSS integration scheme can improve the efficiency of the *high performance* FORTRAN implementation further.

4.4 Coupling with *FEM*

The *WBM* exhibits better convergence properties than the *FEM* as is demonstrated in section 3. However, the applicability of the *WBM* is limited since the high computational efficiency only appears for *acoustic* systems of moderate geometrical complexity. Otherwise, the division in many small subdomains is required by means of domain decomposition (see section 4.1), which increases the computational efforts. The *FEM* exhibits almost no restrictions with respect to the geometrical features of a system.

In order to benefit from the advantageous features of both methods, which are the wide application range of the *FEM* and the high convergence rate of the *WBM*, the coupling between both prediction tools is proposed [11]. The basic idea is to replace those parts of the *finite element* model, which have a simple geometrical shape, by much smaller *wave models*. The resulting hybrid model has less *DOF's*. This allows a further model refinement of the *finite element* part, which leads to an improved accuracy.

The theoretical background of the proposed coupled approach is given in [11] and will be omitted here. The preliminary results of this approach applied to a *2D acoustic* problem with a non-convex geometrical shape are promising. The *hybrid* model suffers less from pollution errors than a full *finite element* model with the same mesh size as the *finite element* part of the *hybrid* model. Although the research on the coupled approach is initiated recently, the preliminary results already indicate that it has the potential to cover the mid-frequency range for practical engineering problems.

5 Conclusions

First, the theoretical background of the *WBM*, applied to *2D uncoupled acoustic* problems, has been explained. The *wave model* is derived based on both the *WR* formulation and the *LS* formulation. The latter approach is less efficient certainly near the first resonance peaks in the pressure *FRF's*.

This paper demonstrates the computational efficiency of the method for a *2D uncoupled acoustic* benchmark problem. A high accuracy compared to the *finite element* results is observed qualitatively by the comparison of the pressure *FRF's*. The *WBM* does not suffer from pollution errors like the *FEM* does. A more detailed convergence analysis shows the better convergence properties of the *WBM* with

respect to the model sizes. Furthermore, the *high performance* FORTRAN implementation is also more efficient with respect to the CPU times.

The remainder of the paper discusses some research topics of the conceptual development of the *WBM*. Most attention goes to the domain decomposition. First the use of this approach is motivated, followed by a brief overview of the theoretical background. The accuracy of the domain decomposition is verified on a *2D acoustic L-shaped* benchmark problem both by qualitative means (visual inspection) and by a detailed convergence analysis. The conclusion is that also for this considered problem the *WBM*, using domain decomposition, exhibits better convergence properties than the *FEM*. Furthermore, three extensions of the current wave function set are proposed, the replacement of the GAUSS integration procedure by analytical solution functions is considered and finally the coupling with the *FEM* is discussed. All new developments allow the improvement of the efficiency of the *high performance* FORTRAN implementation of the *WBM* in the future.

Acknowledgements

The research of B. van Hal is financed by a scholarship of the Institute for the Promotion of Innovation by Science and Technology in Flanders (Belgium) (IWT). W. Desmet is a Postdoctoral Fellow of the Fund for Scientific Research Flanders (FWO). The research of ACC is carried out with the support and funding of AVL List GmbH and MAGNA STEYR in Graz. Furthermore, the project is funded by the Austrian government, the government of Styria and the city of Graz.

References

[1] O.C. Zienkiewicz, R.L. Taylor *The Finite Element Method - Vol. 1: Basic formulation and linear problems*, fourth edition, McGraw-Hill, London, UK (1989).

[2] O.C. Zienkiewicz, R.L. Taylor, *The Finite Element Method - Vol. 2: Solid and Fluid Mechanics, Dynamics and Non-Linearity*, fourth edition, McGraw-Hill, London, UK (1991).

[3] W. Desmet, *A wave based prediction technique for coupled vibro-acoustic analysis*, PhD thesis, K.U.Leuven, Leuven (1998).

[4] E. Trefftz, *Ein Gegenstück zum Ritzschen Verfahren*, in *Proceedings of the 2nd Int. Congr. on Appl. Mech.*, Zürich (1926), pp. 131-137.

[5] *SYSNOISE Rev 5.5 Online User's Manual*, LMS International, Leuven.

[6] F. Ihlenburg, *Finite Element Analysis of Acoustic Scattering*, volume 132 of *Applied Mathematical Sciences*, Springer-Verlag New York, Inc. (1998).

[7] A. Hepberger, H.-H. Priebsch, W. Desmet, B. van Hal, P. Sas, *Application of the Wave Based Method for the Steady-state Acoustic Response Prediction of a Car Cavity in the Mid-frequency Range*, in *Proceedings of ISMA2002*, Leuven (2002).

[8] B. van Hal, W. Desmet, B. Pluymers, P. Sas, D. Vandepitte, *Improving the Wave Based Method for the Steady-state Dynamic Analysis of Acoustic Systems*, in *Proceedings of ICSV 9*, Orlando, Florida (2002).

[9] C.F. Gerald, P.O. Wheatley, *Applied Numerical Analysis*, Addison-Wesley Publication Company, fourth edition (1989).

[10] B. van Hal, W. Desmet, D. Vandepitte, P. Sas, *Application of the Efficient Wave Based Prediction Technique for the Steady-state Dynamic Analysis of Flat Plates*, in *Proceedings of ISMA25*, Leuven (2000), pp. 607-614.

[11] B. van Hal, W. Desmet, D. Vandepitte, P. Sas, *A Coupled Finite Element - Wave Based Approach for the Steady-State Dynamic Analysis of Coupled Structural-Acoustic Systems*, in *Proceedings of WCCM V*, Vienna (2002), http://wccm.tuwien.ac.at.